Coherence dynamics of two-mode condensates in asymmetric potentials

M. Jääskeläinen and P. Meystre
Department of Physics and College of Optical Sciences, The University of Arizona, Tucson, Arizona 85721, USA
(Received 26 August 2005; published 3 January 2006)

Detection of weak forces with an accuracy beyond the standard quantum limit holds promise both for fundamental research and for technological applications. Schemes involving ultracold atoms for such measurements are now considered to be prime candidates for increased sensitivity. In this paper we use a combination of analytical and numerical techniques to investigate the possible subshot-noise estimation of applied force fields through detection of coherence dynamics of Bose-condensed atoms in asymmetric double-well traps. Following a semiclassical description of the system dynamics and fringe visibility, we present numerical simulations of the full quantum dynamics that demonstrate the dynamical production of phase squeezing beyond the standard quantum limit. Nonlinear interactions are found to limit the achievable amount to a finite value determined by the external weak force.

DOI: 10.1103/PhysRevA.73.013602 PACS number(s): 03.75.Be, 03.65.Ge, 05.60.Gg

I. INTRODUCTION

The detection of weak forces with an accuracy beyond the standard quantum limit holds promise both for fundamental research and for technological applications. An essential step in achieving this goal is the availability of nonclassical matter-wave sources, as can be generated in optical lattices and multiwell traps. In particular, several studies have been devoted to the analog of spin squeezing [1] in two-mode condensates, both theoretically [2–4] and experimentally [5], and this effect holds promise of increased accuracy in interferometry [6,7]. In related work, the semiclassical dynamics of these systems, which is amenable to a Gross-Pitaevskii treatment analogous to that of Josephson junctions [8], was studied in particular in Refs. [9,10].

Double-well systems such as recently realized experimentally [11] also represent a particularly simple situation to investigate the competition between two-body interactions and quantum tunneling. They already contain much of the physics known to take place in optical lattices, in particular the transition from a Bosonic superfluid to a Mott insulator characterized by significant number squeezing [12–14]. Recent experiments on condensates in optical lattices indicate that these properties make them suitable for the precision measurements of weak applied forces [15,16]. In particular, the so-called "contrast resonances" that appear when these forces modify the potential have been proposed as a sensitive tool to measure these forces.

The dynamics of quantum-degenerate Bosonic systems in double wells (or lattices) depends, however, rather sensitively on the rate at which the potential is changed. For example, a recent study showed that nonadiabaticity can limit the amount of achievable squeezing [17] in optical lattices. Other studies focused on the loading of condensates into lattices [18–20] and the subsequent collapse-revival dynamics, as well as other nonequilibrium situations such as the dynamics of the superfluid state [21,22]. Following the recent experiments of Ref. [23] we also investigated the coherence dynamics in symmetric double-well potentials after sudden changes [24].

In this paper we extend these results to the study of Bose-Einstein condensates in *asymmetric* double-well potentials subjected to sudden changes, and assess the potential use of characteristic signatures of their dynamics to the detection of weak forces. We concentrate on observable quantities such as fringe visibility and phase noise, that is, on the dynamics of the coherences of the matter-wave field, both first and second order, as functions of holding time after a sudden change of the Hamiltonian parameters. We rely on the combination of a semiclassical approximation and of a Bloch-sphere quasiprobability representation to achieve a simple geometrical interpretation of our results. For the problem at hand, the Husimi quasidistribution on the Bloch sphere [24,25] is particularly convenient.

The paper is organized as follows: Sec. II establishes the mathematical framework and derives a formula for the fringe visibility in interference experiments. In Sec. III we apply a semiclassical approximation and derive conditions under which the visibility of the interference fringes vanishes temporarily, thereby providing an intuitive understanding of the "contrast resonances" observed by Kasevich and co-workers. Section IV gives selected results from exact quantum-mechanical simulations for varying particle numbers and Hamiltonian parameters, and investigates the applicability of the semiclassical model by comparison with the exact numerics. This section concludes with a discussion of the application of the system dynamics to the detection of weak forces. Section V investigates possibilities for subshot-noise performance, and Sec. VI is a summary and outlook.

II. MODEL

Provided that excitations to higher states can be neglected, the field operator describing a Bose-condensed gas in an asymmetric double-well trap can be expressed as the superposition of a "right" and a "left" mode as

$$\hat{\Psi}(x) = \hat{a}_L \varphi_L(x) e^{i(\theta/2)} + \hat{a}_R \varphi_R(x) e^{-i(\theta/2)}, \tag{1}$$

where $\varphi_{L/R}(x)$ are mode functions [26], taken to have a relative phase θ, that are spatially localized in the two potential

wells. For sufficiently harmonic potentials the mode functions can be taken to be approximately Gaussian [4]. In this two-mode approximation the condensate Hamiltonian is

$$\hat{H} = \frac{\Delta E}{2}[\hat{a}_L^\dagger \hat{a}_R + \hat{a}_R^\dagger \hat{a}_L] + g[\hat{a}_L^{\dagger 2}\hat{a}_L^2 + \hat{a}_R^{\dagger 2}\hat{a}_R^2] + \frac{\kappa}{2}[\hat{a}_L^\dagger \hat{a}_L - \hat{a}_R^\dagger \hat{a}_R], \tag{2}$$

where we have introduced the tunneling energy

$$\Delta E = \int_{-\infty}^{\infty} dx \varphi_L(x)\left(-\frac{\hbar^2}{2M}\nabla^2 + V(x)\right)\varphi_R(x), \tag{3}$$

the two-body interaction

$$g = a_0 \int_{-\infty}^{\infty} dx |\varphi_{L/R}(x)|^4, \tag{4}$$

with a_0 the two-body coupling constant, and

$$\kappa = f_{\mathrm{ex}} \int_{-\infty}^{\infty} \varphi_L(x) x \varphi_R(x) dx, \tag{5}$$

where f_{ex}, assumed to be negative, is an unknown external field gradient applied to the condensate and to be detected.

This two-mode problem is conveniently reexpressed in the Schwinger angular-momentum representation of Bosonic operators [27]. We proceed by introducing the angular momentum operators

$$\hat{J}_z = \frac{1}{2}(\hat{a}_L^\dagger \hat{a}_L - \hat{a}_R^\dagger \hat{a}_R), \tag{6}$$

$$\hat{J}_y = \frac{1}{2i}(\hat{a}_L^\dagger \hat{a}_R - \hat{a}_R^\dagger \hat{a}_L), \tag{7}$$

$$\hat{J}_x = \frac{1}{2}(\hat{a}_L^\dagger \hat{a}_R + \hat{a}_R^\dagger \hat{a}_L), \tag{8}$$

which can be thought of as the orthogonal components of a Bloch vector of length $N/2$. We then express the state of the matter-wave field in terms of eigenstates $|J,m\rangle$ of the operators $\hat{J}^2$ and $\hat{J}_z$, where

$$\hat{J}^2 = \hat{J}_x^2 + \hat{J}_y^2 + \hat{J}_z^2, \tag{9}$$

with

$$\hat{J}^2|J,m\rangle = \hbar^2 J(J+1)|J,m\rangle, \tag{10}$$

$$\hat{J}_z|J,m\rangle = \hbar m|J,m\rangle = \frac{\hbar}{2}(n_L - n_R)|J,m\rangle, \tag{11}$$

and $J=N/2$, $m=-J,-J+1,\ldots,J$.

In the angular momentum representation the Hamiltonian (2) reads, apart from a physically irrelevant function of the total angular momentum eigenvalue J,

$$\hat{H} = 2g\hat{J}_z^2 + \Delta E \hat{J}_x + \kappa \hat{J}_z. \tag{12}$$

This Hamiltonian is known to produce spin squeezing [1].

We consider the situation where the detection of the atomic field is carried out after the transverse trap is rapidly switched off and the atoms undergo a stage of ballistic expansion. During that stage the stationary mode functions $\varphi_{L/R}(x)$ are replaced by freely expanding Gaussians that are centered around the minima $x=\pm d$ of the potential at the time of release,

$$\varphi_{L/R}(x,t) = \{2\pi\Delta x^2[1 + i\omega(t - t_{\mathrm{exp}})]\}^{-1/4} \times \exp\left(-\frac{(x \pm d)^2}{4\Delta x^2[1 + i\omega(t - t_{\mathrm{exp}})]}\right). \tag{13}$$

Here Δx is the initial width of the Gaussians and t_{exp} is the time at which the confining potential is turned off. At the end of that stage, the spatial density of the condensate is

$$\begin{aligned}\langle G_1(x,t,\theta)\rangle &= \langle \hat{\Psi}^\dagger(x)\hat{\Psi}(x)\rangle \\ &= \langle \hat{n}_L(t)\rangle|\varphi_L(x,t)|^2 + \langle \hat{n}_R(t)\rangle|\varphi_R(x,t)|^2 \\ &\quad + \varphi_L^*(x,t)\varphi_R(x,t)\exp(-i\theta)\langle \hat{J}_+(t)\rangle \\ &\quad + \varphi_L(x,t)\varphi_R^*(x,t)\langle \hat{J}_-(t)\rangle\exp(+i\theta),\end{aligned} \tag{14}$$

resulting in an interference pattern with visibility

$$V = \frac{\max\langle G_1(0,t,\theta)\rangle - \min\langle G_1(0,t,\theta)\rangle}{\max\langle G_1(0,t,\theta)\rangle + \min\langle G_1(0,t,\theta)\rangle}. \tag{15}$$

For Gaussian mode functions (and other suitably symmetric functions) maxima or minima of the density profile are found at $x=0$ when

$$\frac{\partial\langle G_1(0,t,\theta)\rangle}{\partial\theta} = |\varphi(0,t)_{L/R}|^2[\langle \hat{J}_y(t)\rangle\cos\theta - \langle \hat{J}_x(t)\rangle\sin\theta] = 0, \tag{16}$$

where we have used $\varphi_L(0,t)=\varphi_R(0,t)$. Equation (16) gives for the phase angle

$$\tan\theta = \frac{\langle \hat{J}_y(t)\rangle}{\langle \hat{J}_x(t)\rangle}, \tag{17}$$

and after some trigonometry

$$\sin(\theta) = \frac{\langle \hat{J}_y\rangle}{\sqrt{\langle \hat{J}_x\rangle^2 + \langle \hat{J}_y\rangle^2}}. \tag{18}$$

If the density $\langle G_1\rangle$ is maximal for the angle θ, it is minimal for $\theta\pm\pi$, and we have

$$\begin{aligned}&\max\langle G_1(0,t,\theta)\rangle \\ &\quad = |\varphi(0,t)|^2\{N + 2[\langle \hat{J}_x(t)\rangle\cos(\theta) + \langle \hat{J}_y(t)\rangle\sin(\theta)]\}, \\ &\min\langle G_1(0,t,\theta)\rangle \\ &\quad = |\varphi(0,t)|^2\{N - 2[\langle \hat{J}_x(t)\rangle\cos(\theta) + \langle \hat{J}_y(t)\rangle\sin(\theta)]\}.\end{aligned} \tag{19}$$

Using these results together with Eqs. (17) and (18) in the definition (15), we arrive at

$$V(t) = \sqrt{\left(\frac{\langle \hat{J}_x(t)\rangle}{J}\right)^2 + \left(\frac{\langle \hat{J}_y(t)\rangle}{J}\right)^2}. \tag{20}$$

In the angular momentum representation, the fringe visibility is therefore given by the centroid of the quantum state, projected onto the $\hat{J}_x$-$\hat{J}_y$ plane. From Eq. (20) the visibility disappears at those times when

$$\langle \hat{J}_x(t)\rangle = \langle \hat{J}_y(t)\rangle = 0, \tag{21}$$

i.e., either when the distribution is completely polarized or when the phase uncertainty is total. In addition, our derivation shows that the external phase cancels the relative phase of the quadrature components $\hat{J}_x$ and $\hat{J}_y$ in the case of extremal values of the density. Equivalently we can think of the external phase as a rotation of the Bloch sphere around $\hat{J}_z$, as such actions are generated by this component of the pseudospin.

III. SEMICLASSICAL DYNAMICS

In recent experiments by Kasevich and co-workers [15], a condensate subject to an (in principle unknown) external force was prepared in a squeezed state of an optical lattice, whose depth was then switched rapidly to the strongly interacting regime, but still far from the Mott insulator regime. After a variable holding time, the trapping potential was turned off, the condensate visibility was observed after free ballistic expansion, and the dependence of the visibility on the holding time was then used to determine the external force.

Motivated by these results, we investigate the dynamics of the fringe visibility after a rapid change of either the well depth or the two-body interaction energy in a two-well system. We note at the outset that the time scale over which these changes occur cannot be arbitrarily short, as the dynamics of the system has to remain adiabatic with respect to the external mode functions of the confining potential in order for the two-mode model to hold. Indeed, the two-mode approximation is known to be valid provided that the interaction energy Ng is small compared to the energy separation $\hbar\omega$ between the trap levels of the individual traps, and in addition, the spatial mode functions of particles localized on each side of the double well are only well described by shifted Gaussians provided that the interwell tunneling energy ΔE is much smaller than their frequencies, which are also of order $\hbar\omega$ [26]. Finally, the two-mode description also requires that the double-well asymmetry is small compared with the level spacing $\kappa \ll \hbar\omega$ [33]. Provided that these three conditions are met, it is possible to modify the energy ratio G in a time $1/\omega \ll T \ll \hbar/\Delta E, \hbar/gN, \hbar/\kappa$ such that the change is adiabatic with respect to the double well, but practically instantaneous as far as the many-body dynamics is concerned.

We consider first a semiclassical approach, expected to be valid for large particle numbers and weak interaction strengths. This approximation results from the factorization scheme

$$\langle\{\hat{J}_i, \hat{J}_j\}\rangle \approx 2\langle \hat{J}_i\rangle\langle \hat{J}_j\rangle, \tag{22}$$

where {,} is the anticommutator of two operators, which amounts to setting the covariance matrix elements of the angular momentum operators to zero. It should be emphasized that the ansatz, which holds exactly for Gaussian random variables [28], does not necessarily imply that all correlators factorize, i.e.,

$$\langle \hat{J}_i \hat{J}_j\rangle \approx \langle \hat{J}_i\rangle\langle \hat{J}_j\rangle, \tag{23}$$

as would be the case for a fully classical system of point particles. Equation (22) does not assume anything about the angular momentum commutation relations, whereas Eq. (23) violates them. As such, the factorization scheme (22) allows us to handle situations characterized by a moderate amount of squeezing, as further discussed later on.

Introducing the normalized Bloch-vector components

$$s_i \equiv \frac{\langle \hat{J}_i\rangle}{J}, \tag{24}$$

and with Eq. (9), the semiclassical approximation (22) implies that

$$s_x^2 + s_y^2 + s_z^2 = 1 + 1/J \approx 1, \tag{25}$$

which shows that in the limit of large particle numbers the semiclassical dynamics is mapped onto the motion of a point on the surface of a Bloch sphere. In that approximation, the condensate energy, which is given by the expectation value of the (suitably normalized) Hamiltonian

$$\varepsilon \equiv \frac{\langle \hat{H}\rangle}{J\Delta E} = \frac{G}{2}s_z^2 + s_x + Fs_z, \tag{26}$$

where we have introduced the dimensionless interaction strength [4,24]

$$G \equiv \frac{2gN}{\Delta E}, \tag{27}$$

and the dimensionless energy offset between the two wells,

$$F \equiv \frac{\kappa}{\Delta E}. \tag{28}$$

For $G=0$, $F=0$, and also for large enough particle number, the ground state of the two-well system is well approximated by a coherent state, a state for which the semiclassical approximation (22) is particularly well suited. The energy is then proportional to s_x, and is minimal for

$$s_x = -\sqrt{1 + 1/J} \approx -1, \tag{29}$$

from which it follows that

$$s_z = s_y = 0 \tag{30}$$

with corresponding normalized energy

$$\varepsilon_0 = -\sqrt{1 + 1/J} \approx -1. \tag{31}$$

Reference [15] indicates that so-called "contrast resonances," the temporary disappearance of the interference pattern, are

of particular interest for the measurement of weak forces. As we have seen, this happens when the Bloch vector describing the condensate reaches the north pole of the Bloch sphere. At these times, we have semiclassically that $s_x=s_y=0$ and

$$s_z=\sqrt{1+1/J}\approx 1, \tag{32}$$

corresponding to the energy

$$\varepsilon_{NP}=\frac{G}{2}s_z^2+Fs_z\approx\frac{G}{2}+F. \tag{33}$$

The dynamics of the condensate is Hamiltonian and hence its energy is a constant of motion. A given trajectory can therefore connect two points on the Bloch sphere only if they have the same energy. In particular, for the system to evolve from its initial ground state to the north pole we must have

$$G=-\frac{2}{\sqrt{1+1/J}}(F+1)\approx -2(F+1). \tag{34}$$

This is the central result of this paper. It relates the offset of the two potential wells, and hence the external force, to the mean-field energy and the interwell tunneling rate, assumed to be known and controllable in this measurement scheme. Physically, the condition of vanishing visibility amounts to having large enough energy offset to overcome the repulsive interactions between particles, thereby making it possible to accumulate all particles in either of the wells through Josephson tunneling.

The semiclassical equations of motion for the angular momentum components are

$$\frac{ds_x}{dt}=Fs_y+2Gs_ys_z, \tag{35}$$

$$\frac{ds_y}{d\tau}=-s_z+Fs_x+2Gs_xs_z, \tag{36}$$

and

$$\frac{ds_z}{d\tau}=s_y, \tag{37}$$

where time is in dimensionless units

$$\tau\equiv\Delta Et. \tag{38}$$

The approximation (22) implicitly assumes that the dynamics of $\langle\hat{J}_i(t)\rangle$ is not influenced by the cross correlations and dispersions of the pseudospin components. This assumption breaks down when large quantum correlations are present, such as in a superposition state, or in a highly squeezed state. It has been shown that the inclusion of second-order moments as dynamical variables, thus necessitating a factorization of higher-order correlators in order to get a closed set of equations, allows for accurate modeling of the centroid dynamics for slightly longer times [9]. We concentrate in the following on situations where the condensate trajectories reach the north pole. Using Eqs. (26) and (25) together with the initial condition (31), we eliminate both s_x and s_y from Eq. (37), which through separation gives a solution for τ as a function of s_z as

$$\tau(s_z)=\frac{2}{G}\int_0^{s_z}\frac{ds_z'}{\sqrt{s_z'(1-s_z')\left(s_z'^2-\frac{4+G}{G}s_z'+\frac{2+G}{G}\right)}}$$

$$=\frac{4l}{G}[2K(k)+F(\varphi,k)], \tag{39}$$

where $K(k)$ is the complete and $F(\varphi,k)$ is the incomplete elliptical integral of the first kind [29]. The prefactor l of the solution and the amplitude k of the elliptic integrals are given by

$$l=\frac{1}{\sqrt{AB}}, \tag{40}$$

and

$$k=\sqrt{\frac{1-(A-B)^2}{4AB}}, \tag{41}$$

and φ is given implicitly by

$$\cos(\varphi)=\frac{(1-s_z)B-s_zA}{(1-s_z)B+s_zA}, \tag{42}$$

where

$$A=\frac{1}{2}\sqrt{1+2(r_++r_-)+4r_+r_-}, \tag{43}$$

and

$$B=\sqrt{r_+r_-}, \tag{44}$$

$r_\pm$ being roots of the second-order polynomial factor in the denominator of the integrand in Eq. (39),

$$r_\pm=\frac{4+G}{2G}\pm\frac{1}{2G}\sqrt{(G-G_+)(G-G_-)}, \tag{45}$$

with

$$G_\pm=4(1\pm\sqrt{2}). \tag{46}$$

In the absence of two-body interactions, $G=0$, the condensate trajectory is given by rotations of the initial state around the vector $[-1/\sqrt{2},0,1/\sqrt{2}]$, a circle on the Bloch sphere; see Fig. 1. With increasing G the classical trajectories with sufficient energy to reach the north pole of the Bloch sphere become more and more distorted. The value G_+ denotes the largest interaction strength for which the semiclassical trajectories still passes through the north pole.

The zeros in the denominator of the elliptic integral (39) indicate the presence of stationary points along the semiclassical trajectories. For interaction strengths lower than G_+, the integrand has two complex poles, but at $G=G_+$, they become real and the trajectory bifurcates into two separate ones following the appearance of a new stationary point at

$$r_+=\frac{1}{\sqrt{2}}, \tag{47}$$

which corresponds to

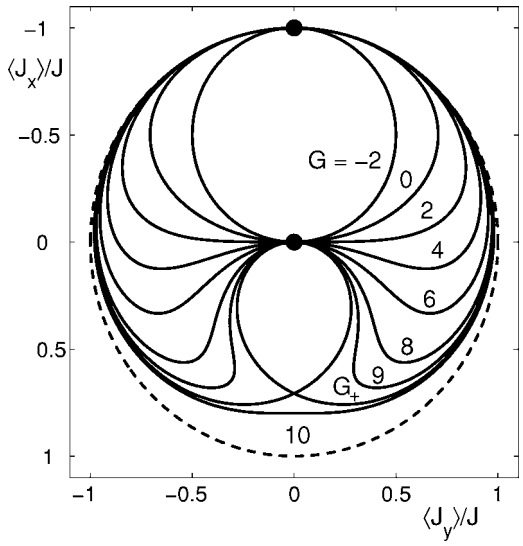

FIG. 1. Semiclassical trajectories with sufficient energy to reach the north pole $\langle \hat{J}_z \rangle = J$. We see that the trajectories become increasingly distorted with stronger interaction. At the value $G_+ \approx 9.657$ [see Eq. (46)] of the interaction strength a bifurcation appears and splits the trajectory through the north pole into two separated ones thus making $s_z = \sqrt{1+1/J}$ inaccessible for the initial condition $s_z = 0$. The outline of the Bloch sphere is shown as a dashed line. The two black dots mark the north pole and the initial state, respectively.

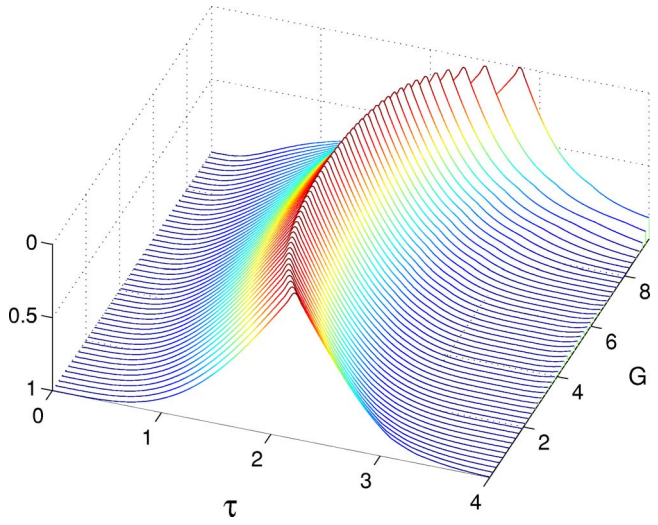

FIG. 2. (Color online) Visibility in the semiclassical limit as a function of dimensionless time and interaction strength G as given by Eq. (39). At the parameter value $G_+ = 4(1+\sqrt{2})$, the time required to reach the north pole ($\langle \hat{J}_z \rangle = J$) goes to infinity due to the presence of a bifurcation.

$$s_x = \frac{1}{\sqrt{2}} \sqrt{1 + \frac{2}{J}} \approx \frac{1}{\sqrt{2}}, \tag{48}$$

and

$$s_y = 0. \tag{49}$$

This bifurcation makes it impossible to reach the north pole from the initial ground state after that point. Figure 2 shows the time dependence of the fringe visibility dynamics as a function of the interaction strength when the energy condition (34) is fulfilled. As the trajectories approach the bifurcation point, the propagation time to reach zero visibility goes to infinity.

Bifurcations are present on the Bloch sphere for all nonzero values of G [10], but they only affect the semiclassical dynamics when any of them crosses the trajectory given by Eq. (39). We also note that the semiclassical trajectories cannot intersect, since they correspond to a conservative Hamiltonian, whereas the quantum-mechanical expectation values, representing the dynamics of a distribution, can intersect and in general do so. It is also worth noting that the semiclassical solutions are periodic in time and thus form closed orbits on the Bloch sphere.

IV. QUANTUM DYNAMICS

In this section we investigate the limitations of the semiclassical description of the dynamics by comparing the visibility dynamics obtained in the previous section with results from exact quantum-mechanical simulations. We also investigate under which conditions the dynamics of the fringe visibility can be used for metrological purposes, such as the determination of weak potential gradients applied to the condensate, with an accuracy beyond the standard quantum limit.

With the Hamiltonian (12) expressed in an angular momentum picture, it is natural and convenient to expand the state of the condensate in terms of the azimuthal quantum number eigenstates

$$|\psi\rangle = \sum_{m=-J}^{J} c_m |J,m\rangle, \tag{50}$$

where $|c_m|^2$ is then the probability for having an atomic population difference of m between the two wells. Since $m \leqslant J$ is bounded, its conjugate variable, the phase difference between the two wells, takes on discrete values θ_m only. Instead of the expansion (50), one can also expand the state of the condensate into so-called relative phase states

$$|\psi\rangle = \sum_{m} c_{\theta_m} |\theta_m\rangle, \tag{51}$$

where [30]

$$|\theta_m\rangle = \frac{1}{\sqrt{2J+1}} \sum_{m'=-J}^{J} \exp(im'\theta_m) |J,m'\rangle, \tag{52}$$

and the discrete relative phases are given by

$$\theta_m = \theta_0 + \frac{2\pi m}{2J+1}, \tag{53}$$

for an arbitrary reference phase θ_0 between the two modes, set equal to zero in the following without loss of generality.

Figure 3 illustrates the quantum dynamics of the condensate both in the relative number basis and in the relative phase representation. This example is for a system initially in

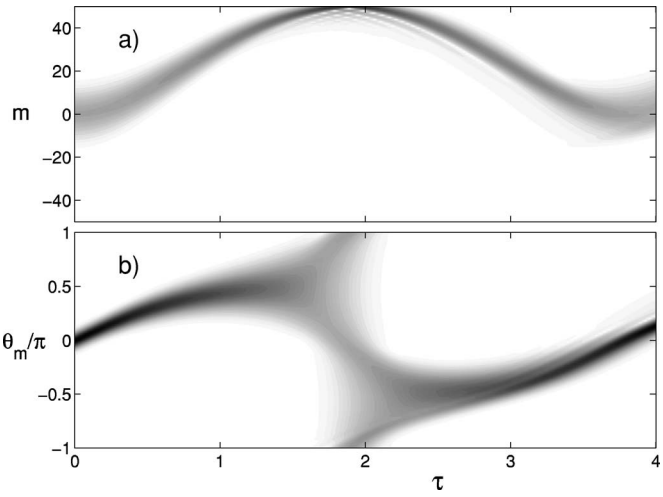

FIG. 3. Density plots of the number (50) and phase distributions (52) versus time. Darker shading corresponds to higher probability density. The dynamics is shown here for $N=100$, $G=2$, $F=-2$. The center of the distribution propagates up to the classical north pole and bounces back, producing interference fringes during the reflection.

the ground state of the noninteracting condensate, corresponding to a symmetric distribution with $m=0$. As the two-body interactions are rapidly switched on to their final value $G=2$, it evolves toward the point $m=J$, corresponding to all particles in one well. The dynamics in the relative number m resembles that of one-dimensional wave packets in anharmonic potentials [24]. When the wave packet reaches the north pole $m=J$, a reflection occurs and interference fringes appear in c_m as a function of m. This occurs at the time of vanishing visibility $V(\tau)$. At that time the relative phase distribution becomes broad as the relative number becomes well defined around $m=J$.

While the example of Fig. 3 corresponds to a situation when the semiclassical approximation holds quite well, it is important to determine when this is the case in general. In order to investigate this point we solved for the exact quantum dynamics associated with the Hamiltonian (12) for the initial coherent state associated with a noninteracting condensate, and rapidly changing the two-body interaction and/or tunneling to satisfy the energy condition (34). The system was then allowed to evolve unitarily until the trap was rapidly turned off and the condensate modes allowed to expand and interfere. The results of these simulations are summarized in Fig. 4 and should be compared with the semiclassical results of Fig. 2. The full quantum simulations coincide with the semiclassical analytical solution in the case of weak interaction strengths, higher particle numbers pushing the validity of the semiclassical description to higher G, as would be intuitively expected.

Section III showed that the disappearance of the visibility ("contrast resonance") at specific times occurs as a result of the energy balance condition (34). This feature thus depends on the precise values of the lattice and condensate parameters, and given that the interaction strength can be tuned, it permits one to determine the energy offset caused by a weak force. In order to investigate this scheme in more detail, we

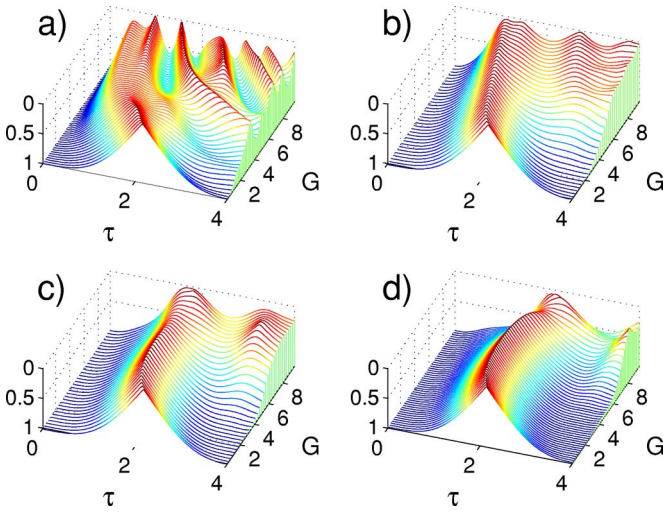

FIG. 4. (Color online) Visibility for the exact quantum-mechanical case as a function of dimensionless time and interaction strength for $N=$(a) 5, (b) 50, (c) 500, and (d) 5000 atoms. The energy balancing condition (34) was used here. For small values of interaction strength G the visibility is well described by the semiclassical approach in Fig. 2 and Eq. (39), while larger values of interaction strength show a breakdown of the semiclassical approach. The regime of validity is extended with increased number of particles.

simulated the quantum dynamics for variable interaction strength while keeping the energy offset constant. The results are shown in Fig. 5, where the visibility dip appears only when the energy balance given by Eq. (34) is satisfied. The visibility peaks sharply around the corresponding value of G, provided, however, that the trajectories remain far from the semiclassical bifurcation, which is the case in cases (a) and (b). In case (c) where the interaction strength is large the

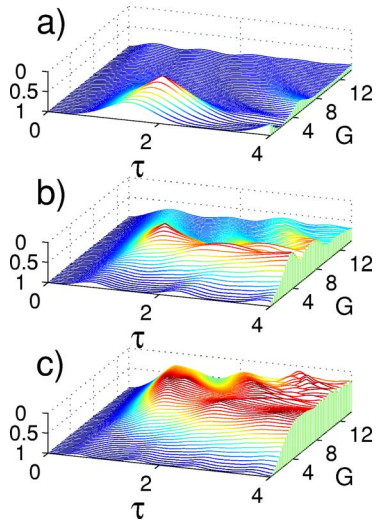

FIG. 5. (Color online) Visibility for the exact quantum-mechanical case for $N=50$ as a function of dimensionless time and interaction strength, for $F=$(a) -2, (b) -4, (c) -6. From Eq. (34) the corresponding values of G are $G=$(a) 2, (b) 6, (c) 10. In (a) and (b) the disappearance of the visibility is a sharp feature, whereas in (c) the peak is smeared out and less distinct.

"resonance" peak is no longer well defined, as its location would fall in the regime where the semiclassical approximation ceases to be valid. This appears to indicate that the application of "contrast resonances" for metrological applications works best in or near the semiclassical regime.

The semiclassical regime is characterized by the fact that the phase space area of the quantum state is small compared with the distances over which the semiclassical energy (26) changes markedly. This does, however, not exclude the presence of quantum correlations in the form of squeezing, a point to which we turn to next.

V. SQUEEZING

The ability to accurately determine applied forces in the present scheme depends on how well the time of vanishing uncertainty can be measured. This in turn depends on both the fluctuations in visibility and on the phase fluctuations. Using Eq. (19), we have for the amplitude of the interference fringes

$$V \propto \max\langle G_1\rangle - \min\langle G_1\rangle \propto \langle \hat{J}_x(t)\rangle\cos(\theta) + \langle \hat{J}_y(t)\rangle\sin(\theta), \tag{54}$$

and for the fluctuations in visibility we get

$$\Delta V(\tau) \propto \Delta\hat{J}_x(t)\cos^2(\theta) + \Delta\hat{J}_y(t)\sin^2(\theta) + [\langle \hat{J}_x(t), \hat{J}_y(t)\rangle - 2\langle J_x(t)\rangle\langle J_y(t)\rangle]\sin(\theta)\cos(\theta). \tag{55}$$

Figure 1 shows that as the trajectories pass through the north pole of the Bloch sphere, they are parallel to the $\hat{J}_y$ axis. As a result $|\langle \hat{J}_x(\tau)\rangle| \ll |\langle \hat{J}_y(\tau)\rangle|$ around the time of vanishing visibility, so that $\cos(\theta)=0$ and

$$\Delta V(\tau) \propto \Delta\hat{J}_y(\tau), \tag{56}$$

i.e., the fluctuations in visibility are entirely due to phase fluctuations. Phase noise is limited by its intrinsic quantum-mechanical contribution and results in a fundamental limit in the determination of weak external forces. The redistribution of the noise in the quadrature components then holds the possibility of increasing the precision in measurements below the shot-noise limit. It is well known that nonclassical correlations in the form of squeezing are induced by nonlinear interactions. For the case at hand, Fig. 3 shows that when the system reaches the north pole the phase distribution is slightly concentrated at the values $\theta_m=0, \pm\pi$, an indication of squeezing created dynamically during the time evolution.

A measure of the squeezing of phase noise relative to its initial value is given by

$$\xi = \frac{\langle \hat{J}_y^2(\tau_{\min})\rangle}{\langle \hat{J}_y^2(0)\rangle}, \tag{57}$$

where $\tau_{\min}$ is the time at which the expectation values of the coherences $\langle \hat{J}_x\rangle$ and $\langle \hat{J}_y\rangle$ equal zero. (Note that decreasing ξ indicates increasing squeezing of the $\hat{J}_y$ component.) This measure does not take into account changes in the total coherence in terms of Bloch vector length, but assumes that the quantum state is fairly well localized on the Bloch sphere. Still, it is a good measure of phase squeezing around $V(\tau_{\min})=0$ under the conditions that we are considering.

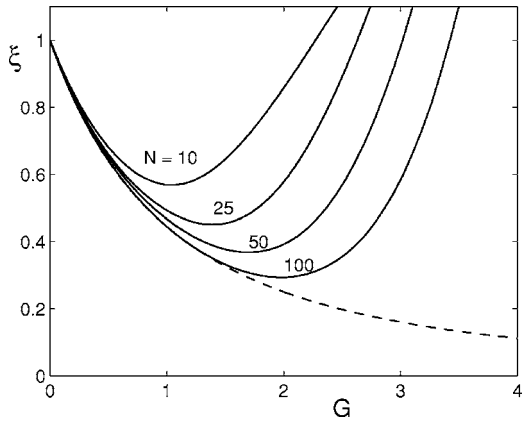

FIG. 6. Squeezing in phase noise, Eq. (57), versus interaction strength for various particle numbers. Dashed line: analytical estimate (63).

Figure 6 shows the squeezing (57) calculated numerically at $\tau_{\min}$ for various particle numbers as a function of the interaction strength G. Squeezing is seen to be present and reaches a minimal value as a function of interaction strength for each particle number.

Quantum dynamics are conveniently described and visualized in terms of phase-space representations [31] such as the Husimi distribution $Q(\varphi,\theta)$ on the Bloch sphere

$$Q(\varphi,\theta) = |\langle \psi(t)|\varphi,\theta\rangle|^2, \tag{58}$$

where the angular Bloch states are given by [32]

$$|\varphi,\theta\rangle = \sum_{m=-J}^{J} \sqrt{\binom{2J}{m+J}}\sin^{J+m}(\theta/2)\cos^{J-m}(\theta/2) \times \exp[-i(J+m)\varphi]|J,m\rangle. \tag{59}$$

The Q function (58) corresponds to the probability distribution of a joint measurement of the difference in particle number together with the relative phase between the condensate modes. As such, the components of its dispersion can be directly associated with experimental noise. Figure 7 gives snapshots of the Q function for $N=100$, $G=2$, and $F=-2$, the situation that corresponds to maximal phase squeezing. The distribution is smeared out along the $\hat{J}_x$ direction as it flows up toward the north pole, resulting in reduced phase noise. At the same time the centroid describes a smooth trajectory well approximated by the semiclassical dynamics of Sec. III.

For larger interaction strengths this picture becomes slightly more complex, as shown in the snapshots of Fig. 8 for the case $G=6$, $F=-4$, $N=100$: the distribution becomes increasingly distorted and also rotates during its propagation. Although squeezing is still present, it no longer reduces the phase fluctuations, as its orientation is no longer along $\hat{J}_y$.

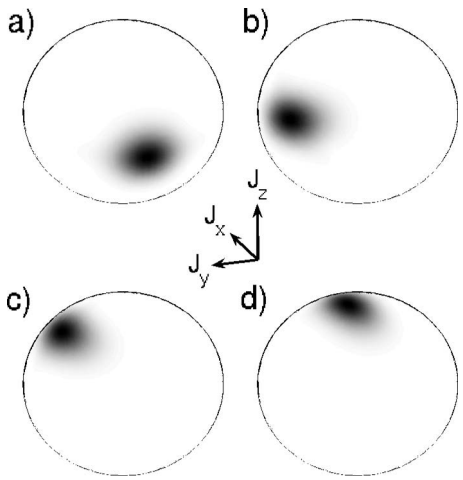

FIG. 7. Q function for $G=2$, $F=-2$, $N=100$, parameters for which maximum squeezing is obtained. Note its elongation elongated as it passes through the north pole. Holding times: $\tau=$(a) 0, (b) 0.6, (c) 1.2, (d) 1.8.

It is possible to derive an estimate of the amount of squeezing that can be achieved dynamically by the Hamiltonian (12). Assuming the dynamics to occur in a minimal uncertainty state, we have for the uncertainties at the north pole of the Bloch-sphere

$$\Delta\hat{J}_x(t)\Delta\hat{J}_y(t) = \frac{1}{2}|\langle\hat{J}_z(t)\rangle|, \tag{60}$$

which allows us to relate the uncertainties in different angular momentum components. If we further assume that these uncertainties relate to energy changes in a linear way, we find for the initial state

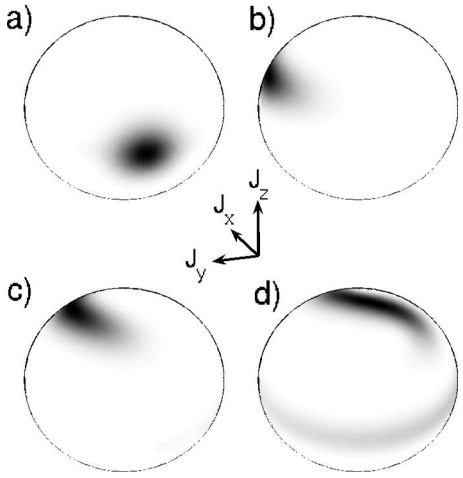

FIG. 8. Q function for $G=6$, $F=-4$, $N=100$. Here the distribution becomes rotated and does not pass through the north pole with its minor axis parallel to $\hat{J}_y$. Also, there is seen to be some twisting in addition to rotation. Holding times: $\tau=$(a) 0, (b) 0.6, (c) 1.2, (d) 1.8.

$$\Delta\varepsilon_0 \approx F\Delta s_z(0) = F\frac{\Delta J_z(0)}{J} = \frac{F}{2\Delta\hat{J}_y(0)}. \tag{61}$$

Similarly, we find at the north pole

$$\Delta\varepsilon_{NP} \approx \Delta s_x = \frac{\Delta J_x(\tau_{\min})}{J} = \frac{1}{2\Delta J_y(\tau_{\min})}, \tag{62}$$

which, assuming $\Delta\varepsilon_0=\Delta\varepsilon_{NP}$, gives for the squeezing parameter (57)

$$\xi = F^{-2} = (1+G/2)^{-2}. \tag{63}$$

This shows that the amount of squeezing which can be created dynamically by the Hamiltonian (12) through evolution to the north pole of the Bloch sphere is limited by the value of the energy offset F, the reason being that squeezing requires redistribution of energy. Figure 6 compares the analytical estimate (63) of the squeezing to the exact numerical results for various particle numbers, and shows a good agreement between the two approaches for small values of G.

Figure 4 shows that increasing the number of particles increases the regime of validity of the semiclassical approximation, whereas Fig. 6 shows that the phase squeezing at the time of disappearing visibility also increases in this limit. While it might appear incorrect that the dynamics of a squeezed state can be described semiclassically, we note that our factorization scheme actually preserves the angular momentum commutation relations, as already mentioned. The fact that in that limit the centroid of the particle distribution is governed by classical equations of motion is a consequence of Ehrenfest's theorem, which states that the expectation values will follow classical trajectories when the width of the distribution is small compared to the scale over which the force fields, the right-hand side of Eqs. (35)–(37), vary appreciably [34]. The only requirement then is that the squeezing is sufficiently weak for the width of the distribution in the antisqueezed direction to remain sufficiently small.

VI. CONCLUSIONS

In this paper we have analyzed the dynamics of Bose-Einstein condensates of interacting atoms trapped in asymmetric double-well potentials whose characteristics are changed suddenly.

An expression for the fringe visibility after ballistic expansion was generalized from earlier work and investigated numerically for cases of interest for applications in metrology, and the dynamics of the fringe visibility was shown to be of potential use for the accurate measurement of small forces.

All the cases described so far have involved repulsive interactions. The dynamics involving attractive interactions has, apart from stability considerations, received comparable little attention. In principle, though, the scheme described in this paper could be implemented also for the case $G<0$. In Fig. 1 the semiclassical trajectories are shown for interaction strengths $-2<G<G_+$. The lower limit corresponds to $F=0$, a completely symmetric double well. In this case the initial

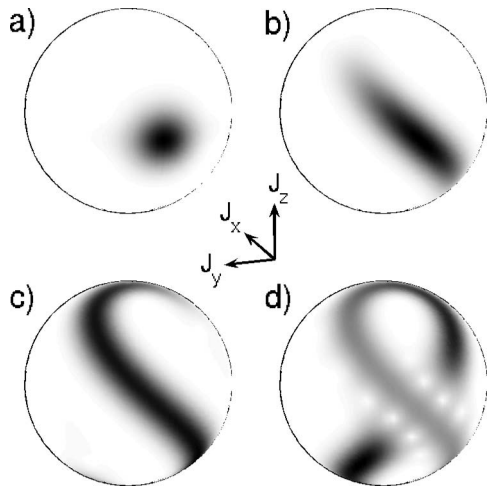

FIG. 9. Quantum dynamics at the onset of a saddle node bifurcation in the semiclassical phase space. Here $N=100$, $G=-2$, $F=0$. Holding times: $\tau=$(a) 0, (b) 1.4, (c) 2.8, (d) 4.2.

state will be centered on a saddle-node bifurcation point. The unstable trajectories pass through the north and south poles and return to the initial point. In the quantum description the distributions are of course smeared out and never completely pointlike for finite particle numbers, resulting in a coherent splitting of the quasidistribution function. Figure 9 illustrates the quantum dynamics at the bifurcation point for $N=100$. The distribution is extended along the semiclassically unstable manifolds through the bifurcation point. After some time the flow of the Q-function returns to the initial centroid and produces interference fringes. It is obvious that under such circumstances the dynamics cannot be modeled using a single semiclassical trajectory, but rather must take the spread in initial distribution into account. A detailed investigation of the dynamics for this situation, although interesting in its own right due to the highly nonclassical features, is not useful for the interferometric schemes considered here and is left for future work.

ACKNOWLEDGMENTS

We thank Ari Tuchman and Mark Kasevich for stimulating discussions and for making their results [15,16] available to us prior to publication. This work was supported in part by the US Office of Naval Research, by the National Science Foundation, by the US Army Research Office, by the National Aeronautics and Space Administration, and by the Joint Services Optics Program.

[1] M. Kitagawa and M. Ueda, Phys. Rev. A **47**, 5138 (1993).
[2] M. J. Steel and M. J. Collett, Phys. Rev. A **57**, 2920 (1998).
[3] J. Javanainen and M. Yu. Ivanov, Phys. Rev. A **60**, 2351 (1999).
[4] M. Jääskeläinen, W. Zhang, and P. Meystre, Phys. Rev. A **70**, 063612 (2004).
[5] C. Orzel, A. K. Tuchman, M. L. Fenselau, M. Yasuda, and M. A. Kasevich, Science **291**, 2386 (2001).
[6] J. F. Corney, G. J. Milburn, and W. Zhang, Phys. Rev. A **59**, 4630 (1999).
[7] J. A. Dunningham and K. Burnett, Phys. Rev. A **70**, 033601 (2004).
[8] S. Raghavan, A. Smerzi, S. Fantoni, and S. R. Shenoy, Phys. Rev. A **59**, 620 (1999).
[9] J. R. Anglin and A. Vardi, Phys. Rev. A **64**, 013605 (2001).
[10] M. E. Kellman and V. Tyng, Phys. Rev. A **66**, 013602 (2002).
[11] M. Albiez *et al.*, Phys. Rev. Lett. **95**, 010402 (2005).
[12] M. P. A. Fisher, P. B. Weichman, G. Grinstein, and D. S. Fisher, Phys. Rev. B **40**, 546 (1989).
[13] D. Jaksch, C. Bruder, J. I. Cirac, C. W. Gardiner, and P. Zoller, Phys. Rev. Lett. **81**, 3108 (1998).
[14] M. Greiner, O. Mandel, T. Esslinger, T. W. Hänsch, and I. Bloch, Nature (London) **415**, 39 (2002).
[15] A. K. Tuchman and M. Kasevich (unpublished).
[16] A. K. Tuchman, Ph.D. thesis, Yale University, 2004.
[17] L. Isella and J. Ruostekoski, Phys. Rev. A **72**, 011601(R) (2005).
[18] J. Plata, Phys. Rev. A **69**, 033604 (2004).
[19] O. Morsch, J. H. Müller, D. Ciampini, M. Cristiani, P. B. Blakie, C. J. Williams, P. S. Julienne, and E. Arimondo, Phys. Rev. A **67**, 031603(R) (2003).
[20] A.-M. Rey, B. L. Hu, E. Calzetta, A. Roura, and C. W. Clark, Phys. Rev. A **69**, 033610 (2004).
[21] A. Polkovnikov, S. Sachdev, and S. M. Girvin, Phys. Rev. A **66**, 053607 (2002).
[22] E. Altman and A. Auerbach, Phys. Rev. Lett. **89**, 250404 (2002).
[23] A. K. Tuchman, C. Orzel, A. Povkolnokov, and M. Kasevich, cond-mat/0504762.
[24] M. Jääskeläinen and P. Meystre, Phys. Rev. A **71**, 043603 (2005).
[25] K. W. Mahmud, H. Perry, and W. P. Reinhardt, Phys. Rev. A **71**, 023615 (2005).
[26] M. Jääskeläinen and S. Stenholm, Phys. Rev. A **68**, 033607 (2003).
[27] G. J. Milburn, J. Corney, E. M. Wright, and D. F. Walls, Phys. Rev. A **55**, 4318 (1997).
[28] I. S. Reed, IRE Trans. Inf. Theory **8**, 194 (1962).
[29] *Handbook of Elliptic Integrals for Engineers and Physicists*, edited by P. F. Byrd and M. D. Friedman (Springer, Heidelberg, 1954).
[30] D. T. Pegg and S. M. Barnett, Phys. Rev. A **39**, 1665 (1989); A. Luis and L. L. Sanchez-Soto, *ibid.* **48**, 4702 (1993).
[31] W. P. Schleich, *Quantum Optics in Phase Space* (Wiley-VCH, Berlin, 2001).
[32] F. T. Arrechi, E. Courtens, R. Gilmore, and H. Thomas, Phys. Rev. A **6**, 2211 (1972).
[33] J. H. Weiner and S. T. Tse, J. Chem. Phys. **74**, 2419 (1981).
[34] L. E. Ballentine, Y. Yang, and J. P. Zibin, Phys. Rev. A **50**, 2854 (1994).